KSME

Springer

Journal of Mechanical Science and Technology 35 (5) 2021

Original Article
DOI 10.1007/s12206-021-0436-0

Keywords:
· Finger-wheeled mechanism
· Modular rope-climbing robot
· Obstacle-crossing
· Optimization calculating method

Correspondence to:
Changlong Ye
sau_robot@163.com

Citation:
Yu, S., Ye, C., Tao, G., Ding, J., Wang, Y. (2021). Design and analysis of a modular rope-climbing robot with the finger-wheeled mechanism. Journal of Mechanical Science and Technology 35 (5) (2021) 2197~2207.
http://doi.org/10.1007/s12206-021-0436-0

Received December 10th, 2020
Revised January 14th, 2021
Accepted January 26th, 2021

† Recommended by Editor
Ja Choon Koo

Design and analysis of a modular rope-climbing robot with the finger-wheeled mechanism

Suyang Yu, Changlong Ye, Guanghong Tao, Jian Ding and Yinchao Wang

School of Mechatronics Engineering, Shenyang Aerospace University, Shenyang, China

Abstract The rope-climbing robot that can cling to a rope for locomotion has been a popular equipment for some inspection applications due to its high flexibility. In this study, a modular rope-climbing robot with the finger-wheeled mechanism is proposed. Due to the ingenious finger-wheeled mechanism and the modular structure, the robot can achieve smooth and quick movement and good capability of obstacle-crossing on the rope and has a high adaptability for different rope environments. On the basis of introducing the robot mechanism, the geometric definitions and descriptions that can present the robot configuration and position relative to the rope are established. Aiming at three typical states during obstacle-crossing, the geometric and force analysis is performed to establish the constraint equations for the robot, and then the simulation is carried out with the optimization calculating method to solve the geometric variables and external forces of the robot that can be used for the robot design work. Finally, the robot prototype is developed based on the design and analysis work, and the experiment is conducted to verify the performance of the robot.

1. Introduction

A rope-climbing robot is one kind of the mobile robot that can cling to a rope for locomotion. Compared with the pole-climbing robot [1, 2] and wall-climbing robot [3, 4], which are also used mainly for some overhead work, a rope-climbing robot can provide more flexibility because it can be deployed simply just by setting up some guide ropes. Nowadays, the rope-climbing robot has been a popular domain with research potential and various applications such as the inspection for power transmission line and suspension bridge [5-7].

In recent decades, a wide variety of rope-climbing robots have been developed, and according to the mechanism being used, these robots can be mainly classified into three types: the leg type, wheel type, and hybrid type. Most of the leg type rope-climbing robots are designed based on the bionics concept. For example, two kinds of rope-climbing robots imitating the ape are developed in Refs. [8, 9], and a rope-climbing robot imitating the sloth-bear is developed in Ref. [10]. These leg type robots have a good adaptability for ropes with different diameter and roughness values, but their movement is usually fluctuating and not quick enough for real applications. Compared to the leg type rope-climbing robot, the wheel type one usually can achieve a smooth and quick movement [11-13], but ordinary wheel mechanisms do not have a good capability for obstacle-crossing, especially for the obstacle vertical to the rope for suspending.

In order to obtain both the smooth and quick movement and good capability of obstacle-crossing, some researchers proposed hybrid type rope-climbing robots which usually adopt the scheme that arranging wheels at the end of some joint arms. For example, some rope-climbing robots with two wheeled arms are developed in Refs. [14-16], and some ones with three or more wheeled arms are developed in Refs. [17-19]. For most of this type robots, the joint arm can be used for crossing the obstacle on the rope, and the end wheel can be used for moving on the rope. At present, the hybrid type rope-climbing robot with joint arms have been used as

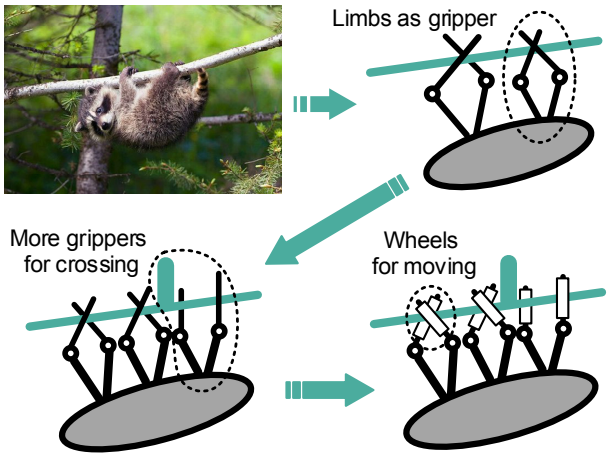

Fig. 1. Concept of finger-wheeled mechanism.

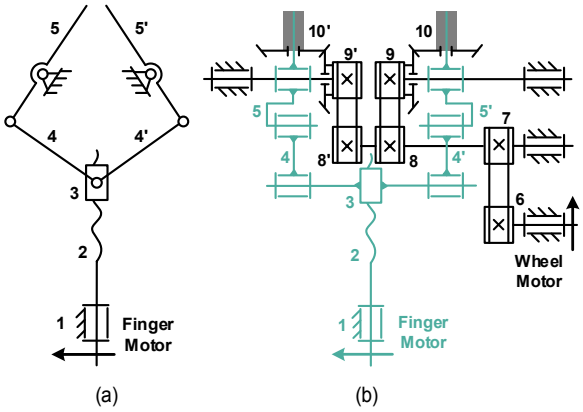

Fig. 2. Schematic diagram of single module (1. Frame, 2. Screw, 3. Slider, 4(4'). Link, 5(5'). Crank as finger, 6-8(8'). Pulley, 9(9'). Pulley with bevel gear, 10(10'). Wheel with bevel gear).

one of the most popular measures for inspection of power transmission line. However, there are still some problems for existing hybrid type rope-climbing robots. For example, the obstacle-crossing mechanism of the robot is usually very complex due to the joint on the arm, and some robots even need counterweight and extra joints for adjusting the body obliquity. Moreover, some robots are very heavy and difficult to be placed on the rope, and only few robots can change the construction for different rope environments.

In view of the above issues, a rope-climbing robot with the ingenious finger-wheeled mechanism, which can be considered as a combination of the bionics concept and traditional wheels, is proposed in this paper. The robot can achieve smooth and quick movement and good capability of obstacle-crossing on the rope with a very simple mechanical structure, and the modular design makes the robot can adapt for different rope environments very well through reconstruction. In order to develop the robot prototype, some geometric and force analysis is performed in this paper, and the simulation results provide a good guidance for the robot design work. Finally, the experiment is conducted to verify the performance of the robot.

2. Robot mechanism

2.1 Concept of finger-wheeled mechanism

The concept of the finger-wheeled mechanism comes from the bionics design of a sloth bear as shown in Fig. 1. The study of the sloth bear in motion shows that the bear uses both pairs of its limbs to climb a branch, and each pair of limbs acts as a gripper. During climbing, only one pair of limbs is used at a time for gripping the branch while the other pair slides over the branch.

When the movement of the sloth bear is used for designing the rope-climbing robot in this study, firstly more pairs of limbs (grippers) are used for a better capability of obstacle-crossing. Moreover, in order to increase the climbing speed, some wheels are added to the end of each limb. Since the appearance of a gripper with two slender wheels is very like fingers of human beings, this novel mechanism is named the finger-wheeled mechanism in this study.

2.2 Mechanism of single module

Based on the concept of the finger-wheeled mechanism, a new-style rope-climbing robot is designed. In order to improve the adaptability of the robot for different rope environments, the modular concept is also used for the mechanical design work. Therefore, each finger-wheeled mechanism, which will act as one gripper, is designed as one module, and its schematic diagram is shown in Fig. 2.

From the schematic diagram it can be seen that the grip action of the finger-wheeled mechanism (open and close of the finger) is realized with a symmetrical crank-slider mechanism as shown in Fig. 2(a). In this crank-slider mechanism, slider 3 is driven by the finger motor through screw 2 to make a translational movement relative to frame 1. Then through link 4 (4'), slider 3 (3') can drive crank 5 (5'), which is also the finger, to make a rock movement relative to frame 1.

The rotation of wheels in the finger-wheeled mechanism is driven with a transmission system consisting of the timing belt and bevel gear as shown in Fig. 2(b). In this transmission system, the wheel motor is used for driving wheel 10 (10') that is mounted on crank 5 (5') through bearings. The timing belt is used to transmit rotational movements from the wheel motor to pulleys 6, 7, 8 (8') and 9 (9') which are all mounted on frame 1, and pulley 9 (9') can drive wheel 10 (10') through a pair of bevel gears. Since the cone distance between the bevel gears 10 (10') and 9 (9') is constant during the rotation of crank 5, driving of the wheel in the mechanism can be achieved for any rotational position of the finger.

Based on the schematic diagram shown in Fig. 2, the mechanical structure of the finger-wheeled mechanism module is designed as shown in Fig. 3.

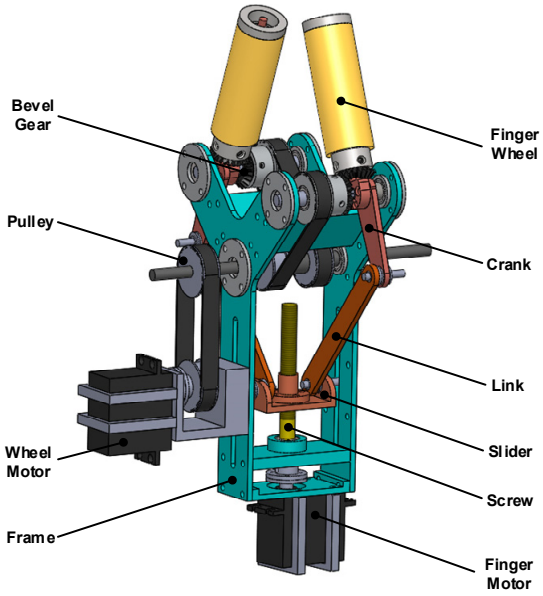

Fig. 3. Mechanical structure of single module.

2.3 Construction of robot

From the mechanical structure of the finger-wheeled mechanism module shown in Fig. 3 it can be seen that, one module can construct a simplest rope-climbing robot. In this robot construction, the finger motor can make the robot grip on the rope, and the wheel motor can make the robot move along the rope. This simplest robot is very suitable for the application that there is no obstacle on the rope, and the light-weight of the robot is the first consideration.

If a better capability of obstacle–crossing is needed, especially the obstacle is vertical to the rope for suspending, more modules are required to construct the robot. Usually, the robot construction with three modules is considered having a good capability of obstacle-crossing, because if one module is off-gripping from the rope for crossing the obstacle, there are still two modules gripping on the rope, and the obliquity of the robot body can be controlled by adjusting rotational angles of the two pairs of fingers gripping on the rope, and this will be very useful for preventing the robot tip-over due to gravity moment and helping the off-gripping module to grip the rope again. Surely, if an obstacle with a large longitudinal dimension is set on the rope, a robot construction with more than three modules can also be selected. In this paper, the analysis work will aim at the robot construction with three finger-wheeled mechanism modules.

The mechanical structure of the robot construction with three finger-wheeled mechanism modules is shown in Fig. 4. In this construction, the frames of three modules are connected with rigid plates. The rotations of three pairs of fingers are controlled by three finger motors, respectively. The rotations of three pairs of wheels mounted on the fingers are controlled by only one motor through a common shaft and two couplers in order to obtain a good synchronicity and simplify the mechanical structure.

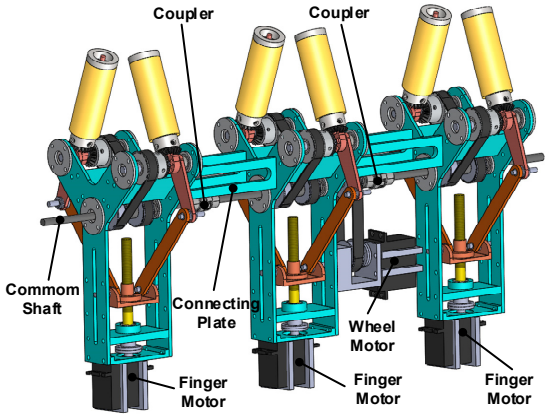

Fig. 4. Construction of the robot with three modules.

The obstacle-crossing process of the robot with three finger-wheeled mechanism modules is shown in Fig. 5. At the beginning of this process, the robot is moving left as the arrow indication with three modules gripping on the rope. When the robot encounters the vertical obstacle, it firstly opens fingers of module 1 to make it off-grip from the rope and then goes on moving to make module 1 cross the obstacle (as shown in Figs. 5(a) and (b)). In this period, the obliquity of the robot body can be controlled by adjusting rotational angles of fingers in modules 2 and 3 for preventing module 3 to upwarp from the rope due to gravity moment. When module 1 has finished crossing (as shown in Figs. 5(b) and (c)), the robot closes fingers of module 1 to make it grip on the rope again. In this period, modules 2 and 3 can also adjust rotational angles of their fingers to lift module 1 to an appropriate vertical position. When module 1 has finished gripping on the rope, the robot opens fingers of module 2 and then goes on moving to make module 2 cross the obstacle (as shown in Figs. 5(c) and (d)). When module 2 has finished crossing (as shown in Figs. 5(d) and (e)), the robot closes fingers of module 2 and opens fingers of module 3. Then the robot goes on moving to make module 3 cross the obstacle (as shown in Figs. 5(e) and (f)), and when module 3 has finished crossing, the robot closes fingers of module 3 to make it grip on the rope again and goes on moving.

From the robot mechanism and obstacle-crossing process it can be seen that, the modular rope-climbing robot with the finger-wheeled mechanism in this study has following advantages.

1) Because the rotation of the finger can be controlled easily, and the area enclosed by a pair of fingers is large enough, the robot can adapt for ropes with different diameter and slope values and be placed on the rope easily.

2) The obliquity of the robot body can be controlled by the rotation of fingers gripping on the rope but not extra joints or motors, so a simpler mechanism is obtained for obstacle-crossing.

3) The robot can adapt for different rope environments and applications by using different number of modules for construction.

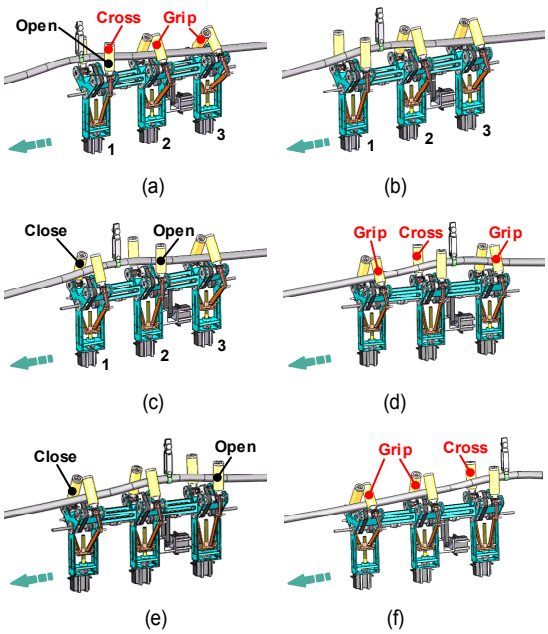

Fig. 5. Obstacle-crossing process of the robot.

3. Geometric definition

In order to analyze the rope-climbing process of the robot, some preliminary geometric definitions and descriptions need to be established to present the robot configuration and position relative to the rope.

3.1 Geometric definition for single module

3.1.1 Mechanism configuration of single module

As previously mentioned, the gripping action of the finger-wheeled mechanism module is realized with a crank-slider mechanism, so firstly, some mechanical constants and variables in the mechanism are defined as shown in Fig. 6. In any module numbered by $i\,(i=1,2,3)$, the mechanism configuration can be described with three mechanical variables, where L_{OAi} is the input displacement of slider A_i; α_i and β_i are rotational angles of link A_iB_i and crank B_iC_i, respectively, and the relation of these three mechanical variables can be written as follows.

$$\begin{cases} L_{AB}\cos\alpha_i + L_{BC}\cos\beta_i - L_{OAi} = 0 \\ L_{AB}\sin\alpha_i - L_{BC}\sin\beta_i - L_{OC} = 0 \end{cases} \tag{1}$$

where L_{AB}, L_{BC}, and L_{OC} are all constant distances between corresponding points of the mechanism shown in Fig. 6.

3.1.2 Rope position for gripping module

In order to describe the relative position between the rope and robot module, firstly, a coordinate system $\{O_i\}$ is defined with module i as shown in Fig. 6. When module i is gripping on the rope, since the rope will contact with the wheel, so the rope position relative to the module, which is described with a variable named the gripping height L_{hi}, can be derived with the vertical coordinate of the rope center z_{Ei}^{Oi} as follows.

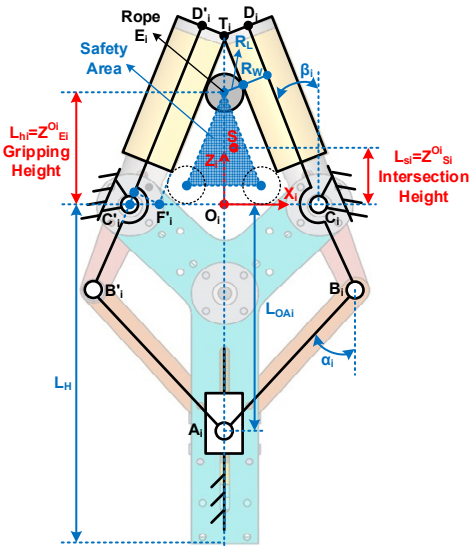

Fig. 6. Geometric definition for single module.

$$L_{hi} = z_{Ei}^{Oi} = f_{Lhi}(\beta_i) = -\left(L_{OC} - \frac{R_W + R_L}{\cos\beta_i}\right)\tan(\beta_i + \pi/2) \tag{2}$$

where R_W and R_L are radii of the robot wheel and rope, respectively, and Eq. (2) shows that the gripping height L_{hi} can be controlled by adjusting the crank angle β_i.

3.1.3 Rope position for crossing module

When module i is off-gripping from the rope for obstacle-crossing, a triangular safety area is defined in plane $X_iO_iZ_i$ according to the area that can be enclosed by the pair of wheels as shown in Fig. 6. The meaning of this definition is that when the module is off-gripping from the rope, if the intersection point between the rope and coordinate plane $X_iO_iZ_i$, which is represented by S_i, is in the safety area, the module can grip the rope again successfully. Since it is considered the rope is arranged in a vertical plane in this paper, the safety area can be transferred to a range for vertical coordinate of the intersection point z_{Si}^{Oi}, which is named as the intersection height L_{si}, as follows.

$$L_{si} = z_{Si}^{Oi} \in \left[\min(L_{hi}),\ \max(L_{hi})\right] = \left[R_L,\ f_{Lhi}(\min(\beta_i))\right] \tag{3}$$

In Eq. (3), the upper limit of L_{si} is the max value of L_{hi} which is corresponding to the min value of β_i represented by $\min(\beta_i)$. This $\min(\beta_i)$ can be solved in the condition that the inner tips of the pair of wheels in plane $X_iO_iZ_i$ touch with each other as shown in Fig. 6. In this condition, the equation for solving $min(\beta_i)$ can be established in triangle $\Delta O_iT_iF_i'$ as follows.

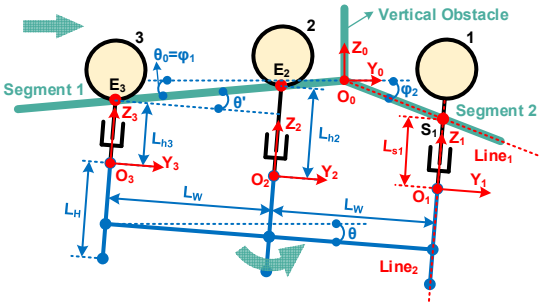

Fig. 7. Geometric definition for obstacle-crossing.

$$\frac{L_{OiFi}}{L_{TiFi}}=\frac{L_{OC}-R_W/\cos\left(\min\left(\beta_i\right)\right)}{L_{CD}-R_W\tan\left(\min\left(\beta_i\right)\right)}=\sin\left(\min\left(\beta_i\right)\right) \tag{4}$$

where L_{OiFi} and L_{TiFi} are side lengths of triangle $\Delta O_iT_iF_i^{'}$ shown in Fig. 6.

3.2 Geometric definition for obstacle-crossing

In order to establish the geometric description for the obstacle-crossing process of the robot, firstly, a simplified rope model is established where the slope angle of each rope segment is represented by φ_i as shown in Fig. 7, and a coordinate system $\{O_0\}$ is defined with the rope. Then the three pairs of wheels of the robot are considered as three circles in plane $Y_0O_0Z_0$, and the gripping point between the robot wheel and the rope is represented by E_i. For example, in the state shown in Fig. 7, modules 2 and 3 are gripping on rope segment 1 at points E_2 and E_3, respectively, and module 1 has crossed the vertical obstacle and is trying to grip the rope segment 2.

During obstacle-crossing (taking the state in Fig. 7 as an example), the obliquity of the robot body represented by θ can be treated as a summation of the basic obliquity θ_0 (inclination of the connecting line between two gripping points E_2 and E_3) and the relative obliquity θ' controlled by gripping heights L_{h2} and L_{h3} of modules 2 and 3. When the obliquity of the robot body is determined, the intersection height L_{s1} of module 1 can be obtained by solving the intersection point of lines 1 and 2 which represent module 1 and rope segment 2, respectively, and if L_{s1} can go into the range in Eq. (3), module 1 can grip the rope successfully.

4. Obstacle-crossing analysis

In this section, the geometric and force analysis for obstacle-crossing on the rope is performed to establish corresponding constraint equations for the robot. These constraint equations can provide a foundation for calculating the geometric variables and external forces exerting on the robot which can be used for guiding the robot design work. The analysis in this section aims at three typical states of the obstacle-crossing process as shown in Fig. 8. Since the spans between gripping points of the robot and the obstacle are not large, the rope shape considering sagging caused by the robot gravity is simplified as a set of folded rope segments in these three states.

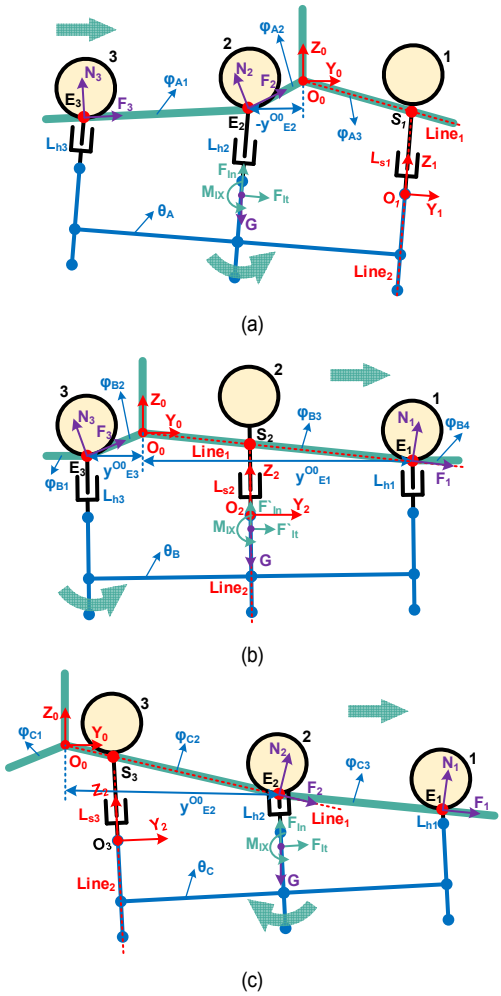

Fig. 8. Obstacle-crossing analysis.

4.1 Geometric analysis

4.1.1 State A

In state A shown in Fig. 8(a), modules 2 and 3 are gripping on the rope, and module 1 has crossed the obstacle and needs to grip the rope again. For this state, two gripping modules are on the same rope segment, so the robot position relative to the obstacle can be described with the coordinates of one gripping point E_2 in $\{O_0\}$ as follows.

$$\left(y_{E2}^{O0},z_{E2}^{O0}\right)=\left(y_{E2}^{O0},y_{E2}^{O0}\tan\varphi_{A2}\right) \tag{5}$$

The obliquity of the robot body θ_A controlled by the gripping heights L_{h2} and L_{h3} can be written as follows.

$$\theta_A=\theta_{A0}+\theta_A^{'}=\varphi_{A1}+\tan^{-1}\left[\left(L_{h3}-L_{h2}\right)/L_W\right] \tag{6}$$

where L_W is the distance between adjacent modules shown in Fig. 7.

The coordinates of the intersection point S_1 in $\{O_0\}$ can be solved with the following equation group.

$$\begin{cases} Line_1: & y_{S1}^{O0}\tan\varphi_{A3}+z_{S1}^{O0}=0 \\ Line_2: & \left(y_{S1}^{O0}-y_{O1}^{O0}\right)+\left(z_{S1}^{O0}-z_{O1}^{O0}\right)\tan\theta_A=0 \end{cases} \tag{7}$$

In Eq. (7), the coordinates of the reference point O_1 in $\{O_0\}$ can be written as follows.

$$\begin{cases} y_{O1}^{O0}=y_{E2}^{O0}+L_{h2}\sin\theta_A+L_W\cos\theta_A \\ z_{O1}^{O0}=z_{E2}^{O0}-L_{h2}\cos\theta_A+L_W\sin\theta_A \end{cases} \tag{8}$$

When the coordinates of point S_1 is solved out, the intersection height of module 1 can be calculated as follows.

$$L_{s1}=L_{h2}-\left[\left(z_{E2}^{O0}-z_{S1}^{O0}\right)\cos\theta_A+\left(y_{S1}^{O0}-y_{E2}^{O0}\right)\sin\theta_A\right] \tag{9}$$

4.1.2 State B

In state B shown in Fig. 8(b), modules 1 and 3 are gripping on the rope, and module 2 has crossed the obstacle and needs to grip the rope again. For this state, since two gripping modules are on different rope segments, so the coordinates of two gripping points E_1 and E_3 in $\{O_0\}$ are used to describe the robot position relative to the obstacle as follows.

$$\begin{cases} \left(y_{E1}^{O0},z_{E1}^{O0}\right)=\left(y_{E1}^{O0},-y_{E1}^{O0}\tan\varphi_{B3}\right) \\ \left(y_{E3}^{O0},z_{E3}^{O0}\right)=\left(y_{E3}^{O0},y_{E3}^{O0}\tan\varphi_{B2}\right) \end{cases} \tag{10}$$

Meanwhile, the coordinates of these two points must satisfy the constraint of the robot dimension as follows.

$$\left(y_{E1}^{O0}-y_{E3}^{O0}\right)\cos\theta_B+\left(z_{E1}^{O0}-z_{E3}^{O0}\right)\sin\theta_B-2L_W=0 \tag{11}$$

The obliquity of the robot body θ_B controlled by the gripping heights L_{h2} and L_{h3} can be written as follows.

$$\begin{aligned}\theta_B=\theta_{B0}+\theta_B^{'}=&\tan^{-1}\left[\left(z_{E1}^{O0}-z_{E3}^{O0}\right)/\left(y_{E1}^{O0}-y_{E3}^{O0}\right)\right]\\&+\tan^{-1}\left[\left(L_{h3}-L_{h1}\right)/\left(2L_W\right)\right]\end{aligned} \tag{12}$$

The coordinates of the intersection point S_2 in $\{O_0\}$ can be solved with the following equation group.

$$\begin{cases} Line_1: & y_{S2}^{O0}\tan\varphi_{A3}+z_{S2}^{O0}=0 \\ Line_2: & \left(y_{S2}^{O0}-y_{O2}^{O0}\right)+\left(z_{S2}^{O0}-z_{O2}^{O0}\right)\tan\theta_B=0 \end{cases} \tag{13}$$

In Eq. (13), the coordinates of the reference point O_2 in $\{O_0\}$ can be written as follows.

$$\begin{cases} y_{O2}^{O0}=y_{E3}^{O0}+L_{h3}\sin\theta_B+L_W\cos\theta_B \\ z_{O2}^{O0}=z_{E3}^{O0}-L_{h3}\cos\theta_B+L_W\sin\theta_B \end{cases} \tag{14}$$

When the coordinates of point S_2 is solved out, the intersection height of module 2 can be calculated as follows.

$$L_{s2}=L_{h3}+\left[\left(z_{S2}^{O0}-z_{E3}^{O0}\right)\cos\theta_B-\left(y_{S2}^{O0}-y_{E3}^{O0}\right)\sin\theta_B\right] \tag{15}$$

4.1.3 State C

In state C shown in Fig. 8(c), modules 1 and 2 are gripping on the rope, and module 3 has crossed the obstacle and needs to grip the rope again. For this state, robot position relative to the obstacle is described with the coordinates of the gripping point E_2 in $\{O_0\}$ as follows.

$$\left(y_{E2}^{O0},z_{E2}^{O0}\right)=\left(y_{E2}^{O0},-y_{E2}^{O0}\tan\varphi_{C2}\right) \tag{16}$$

The obliquity of the robot body θ_C controlled by the gripping heights L_{h1} and L_{h2} can be written as follows.

$$\theta_C=\theta_{C0}+\theta_C^{'}=-\varphi_{C3}+\tan^{-1}\left[\left(L_{h2}-L_{h1}\right)/L_W\right] \tag{17}$$

The coordinates of the intersection point S_3 in $\{O_0\}$ can be solved with the following equation group.

$$\begin{cases} Line_1: & y_{S3}^{O0}\tan\varphi_{C2}+z_{S3}^{O0}=0 \\ Line_2: & \left(y_{S3}^{O0}-y_{O3}^{O0}\right)+\left(z_{S3}^{O0}-z_{O3}^{O0}\right)\tan\theta_C=0 \end{cases} \tag{18}$$

In Eq. (18), the coordinates of the reference point O_3 in $\{O_0\}$ can be written as follows.

$$\begin{cases} y_{O3}^{O0}=y_{E2}^{O0}+L_{h2}\sin\theta_C-L_W\cos\theta_C \\ z_{O3}^{O0}=z_{E2}^{O0}-L_{h2}\cos\theta_C-L_W\sin\theta_C \end{cases} \tag{19}$$

When the coordinates of point S_3 is solved out, the intersection height of module 3 can be calculated as follows.

$$L_{s3}=L_{h2}+\left[\left(z_{S3}^{O0}-z_{E2}^{O0}\right)\cos\theta_C+\left(y_{E2}^{O0}-y_{S3}^{O0}\right)\sin\theta_C\right] \tag{20}$$

4.2 Force analysis

In this section, the robot is considered as a dynamic system, and during rope-climbing, the forces exerting on the robot include the external force from the rope (the normal force N_i and tangential force F_i at each gripping point E_i), the gravity of the robot body G, and the inertial force and moment F_{It} ($F_{It}^{'}$), F_{In} ($F_{In}^{'}$), and M_{IX} as shown in Fig. 8. Moreover, it is assumed that the center of gravity of the robot body is fixed at the midpoint of the length of module 2, and then the force equilibrium equations in plane $Y_0O_0Z_0$, (two equations for resultant force in O_0Y_0 and O_0Z_0 directions and one equation

for resultant force moment relative to a position) are used for establishing the force constraint equations of the robot.

In state A shown in Fig. 8(a), for a given robot position, it is assumed that point E_2 is the rotation center of robot body to lift module 1, and point E_2 is also selected as the reference position of the force moment. Then the force constraint equations can be established as follows.

$$\begin{cases} -N_2\sin\varphi_{A2}+F_2\cos\varphi_{A2}-N_3\sin\varphi_{A1}+F_3\cos\varphi_{A1}+F_{It}\cos\theta_A-F_{In}\sin\theta_A=0 \\ N_2\cos\varphi_{A2}+F_2\sin\varphi_{A2}+N_3\cos\varphi_{A1}+F_3\sin\varphi_{A1}+F_{It}\sin\theta_A+F_{In}\cos\theta_A-G=0 \\ -N_3\left(L_W/\cos\theta_A^{'}\right)-G\left(L_{h2}+L_H/2\right)\sin\theta_A+F_{It}\left(L_{h2}+L_H/2\right)+M_{IX}=0 \end{cases} \tag{21}$$

where L_H is the height of the module shown in Fig. 7. In Eq. (21), the tangential and normal inertial forces F_{It} and F_{In} and inertial moment M_{IX} around point E_2 can be calculated as follows.

$$\begin{cases} F_{It}=m\left(L_{h2}+L_H/2\right)\ddot{\theta}_A \\ F_{In}=m\left(L_{h2}+L_H/2\right)\dot{\theta}_A^2 \\ M_{IX}=J_{E2}\ddot{\theta}_A \end{cases} \tag{22}$$

where m and J_{Ei} are the mass and rotational inertia around point E_i of the robot.

In state B shown in Fig. 8(b), it is assumed that point E_3 is the rotation center of robot body to lift module 2, and point O_0 is selected as the reference position of the force moment. Then the force constraint equations can be established as follows.

$$\begin{cases} N_1\sin\varphi_{B3}+F_1\cos\varphi_{B3}-N_3\sin\varphi_{B2}+F_3\cos\varphi_{B2}+F_{It}^{'}\cos\theta_B-F_{In}^{'}\sin\theta_B=0 \\ N_1\cos\varphi_{B3}-F_1\sin\varphi_{B3}+N_3\cos\varphi_{B2}+F_3\sin\varphi_{B2}+F_{It}^{'}\sin\theta_B-F_{In}^{'}\cos\theta_B-G=0 \\ \left(N_1\cos\varphi_{B3}-F_1\sin\varphi_{B3}\right)y_{E1}^{O0}-\left(N_1\sin\varphi_{B3}+F_1\cos\varphi_{B3}\right)z_{E1}^{O0} \\ +\left(N_3\cos\varphi_{B2}+F_3\sin\varphi_{B2}\right)y_{E3}^{O0}+\left(N_3\sin\varphi_{B2}-F_3\cos\varphi_{B2}\right)z_{E3}^{O0} \\ +\left(F_{It}^{'}-G\sin\theta_B\right)\left[\left(L_{h3}+L_H/2\right)\cos\theta_B-z_{E3}^{O0}\right] \\ +\left(F_{In}^{'}-G\cos\theta_B\right)\left(L_W\cos\theta_B+y_{E3}^{O0}\right)+M_{IX}=0 \end{cases} \tag{23}$$

In Eq. (23), for the convenience of calculating, the inertial force is decomposed along O_2Y_2 and O_2Z_2 (represented by $F_{It}^{'}$ and $F_{In}^{'}$) but not the tangential and normal directions relative to the rotation center E_3, and the inertial force and moment can be calculated as follows.

$$\begin{cases} F_{It}^{'}=m\left[\left(L_{h3}+L_H/2\right)\ddot{\theta}_B-L_W\dot{\theta}_B^2\right] \\ F_{In}^{'}=m\left[L_W\ddot{\theta}_B+\left(L_{h3}+L_H/2\right)\dot{\theta}_B^2\right] \\ M_{IX}=J_{E3}\ddot{\theta}_B \end{cases} \tag{24}$$

In state C shown in Fig. 8(c), it is assumed that point E_2 is the rotation center of robot body to lift module 3, and point E_2 is also selected as the reference position of the force moment. Then the force constraint equations can be established as Eq. (25), and the calculation of the inertial force and moment is the same with Eq. (22).

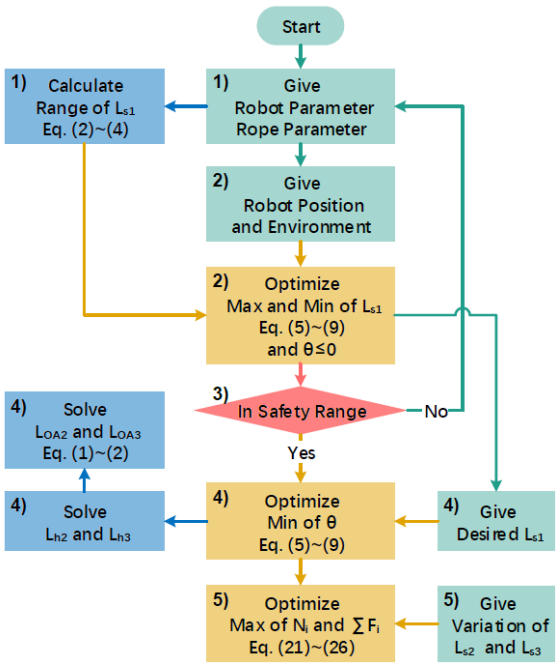

Fig. 9. Simulation flow for state A.

$$\begin{cases} N_1\sin\varphi_{C3}+F_1\cos\varphi_{C3}+N_2\sin\varphi_{C2}+F_2\cos\varphi_{C2}+F_{It}\cos\theta_C-F_{In}\sin\theta_C=0 \\ N_1\cos\varphi_{C3}-F_1\sin\varphi_{C3}+N_2\cos\varphi_{C2}-F_2\sin\varphi_{C2}+F_{It}\sin\theta_C+F_{In}\cos\theta_C-G=0 \\ N_1\left(L_W/\cos\theta_C^{'}\right)-G\left(L_{h2}+L_H/2\right)\sin\theta_C+F_{It}\left(L_{h2}+L_H/2\right)+M_{IX}=0 \end{cases} \tag{25}$$

Meanwhile, since the direction of the normal force from the rope N_i can only be towards the robot wheel, and the tangential force from the rope F_i cannot exceed the friction limit between the rope and robot wheel, two other constraints are established as follows.

$$N_i\geq 0,\quad \left|F_i/N_i\right|\leq\mu \tag{26}$$

where μ is the max frictional coefficient between the rope and robot wheel.

5. Simulation

5.1 Simulation flow

In the simulation, the optimization computing method based on the established constraints is used to obtained the results that can guide the robot design work [20]. The simulation also aims at the three typical states of the robot for obstacle-crossing in Sec. 4. The simulation flow of state A is shown in Fig. 9, and the work in each step of the flow is as follows.

1) **Step 1**: The robot and rope parameters are given firstly, and then the safety range of the intersection height L_{s1} is calculated with Eqs. (2)-(4);

Table 1. Robot and rope parameters in simulation.

L_{AB}	90 mm	L_H	162 mm	μ	0.3
L_{BC}	44 mm	L_W	114 mm	m	5 kg
L_{OC}	42 mm	R_W	12 mm	J_{E2}	0.15 kgm^2
L_{CD}	92 mm	R_L	4 mm	$J_{E1(3)}$	0.22 kgm^2

Table 2. Robot position and environment parameters in simulation.

State A	φ_{A1}	φ_{A2}	φ_{A3}	y_{E2}^{O0}
	2°	15°	5°	-70 mm ~ -50 mm
State B	φ_{B1}	φ_{B2}	φ_{B3}	y_{E3}^{O0}
	2°	15°	10°	-70 mm ~ -50 mm
State C	φ_{C1}	φ_{C2}	φ_{C3}	y_{E2}^{O0}
	5°	10°	2°	210 mm ~ 230 mm

2) **Step 2**: The slope angle of each rope segment and the robot position relative to the rope is given, and then the max and min values of L_{s1}, which is controlled by the gripping heights L_{h2} and L_{h3}, are obtained by optimization with Eqs. (5)-(9) (In the step, the constraint $\theta \le 0$ is added for preventing module 3 to upwarp from the rope due to the gravity moment);

3) **Step 3**: If the extreme range covered by the max and min values of L_{s1} can intersect the safety range of L_{s1}, the simulation will continue, otherwise the robot parameters need to be redesigned;

4) **Step 4**: A desired value of L_{s1} is given (The rule is that the given value should be in the extreme range obtained in step 2 and as close to the mid-point of the safety range obtained in step 1 as possible.), and then the min value of θ is optimized with Eqs. (5)-(9), and the corresponding values for L_{h2} and L_{h3} are obtained, and the input displacements of the mechanism L_{OA2} and L_{OA3} are calculated with Eqs. (1) and (2);

5) **Step 5**: With a determined robot position, the variation of L_{h2} and L_{h3} that can lift module 1 is given, and the max values of external forces N_2, N_3, and (F_2+F_3) (Because all the tangential forces are supplied by one motor, a summation is used here.) in this lift process are obtained, respectively by optimization with Eqs. (21)-(26).

The simulation flow of states B and C are the same with that of state A, but there are some differences in the optimization process as follows.

1) In step 2, when optimizing the max and min values of the intersection height L_{si}, the constraint $\theta \ge 0$ is used in state C for preventing module 1 to upwarp from the rope due to the gravity moment.

2) In step 4, when solving the gripping height L_{hi}, the optimization for the max value of θ is used in state C, and in state B, $\theta = 0$ is given directly.

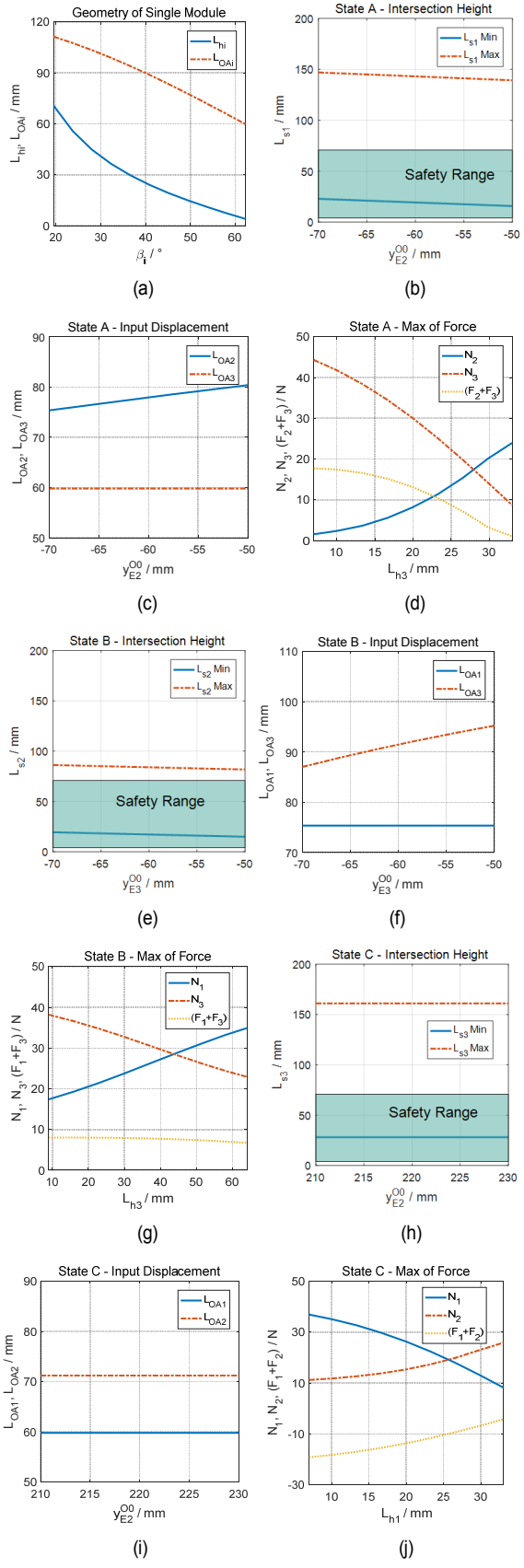

Fig. 10. Simulation results.

5.2 Simulation parameters and results

In the simulation, the robot and rope parameters are given in Table 1, and the robot position and environment parameters are given in Table 2. The simulation is performed on the MATLAB platform, and the results are shown in Fig. 10.

In Fig. 10(a), the variations of gripping height L_{hi} and input displacement L_{OAi} with the crank angle β_i are obtained, wherein the extreme values of L_{hi} can determine the safety range of the intersection height L_{si}, and the range of L_{OAi} can guide the mechanical design work.

In Figs. 10(b), (e) and (h), the variations of the extreme values of the intersection height L_{si} with the robot position for states A, B, and C are obtained, and the results show that during obstacle-crossing, the extreme ranges covered by the max and min values of L_{si} all intersect the safety range (painted with green color), and this means the crossing module can grip the rope again by adjusting the gripping height of the gripping module, and the robot can perform the obstacle-crossing process with the given robot and environment parameters successfully.

In Figs. 10(c), (f) and (i), the variations of the input displacements of the gripping module L_{OAi} with the robot position for states A, B, and C are obtained, and this result can be used for the future robot control work.

In Figs. 10(d), (g) and (j), the variations of the max values of the external forces exerting on the robot N_i and $\sum F_i$ with the gripping height L_{hi} for states A, B, and C are obtained. Since the force analysis aims at the dynamic lift process of the crossing module, in these three figures, the robot position is fixed at the midpoint of the range in Table 2, and the variation velocity of L_{hi} for the gripping module is set 10 mm/s. The final results can be used for mechanical structure and driving system design of the robot.

6. Experiment

Based on the design and analysis work, a robot prototype constructed with three finger-wheeled mechanism modules is developed with the same parameters as that in the simulation, and a rope-climbing experiment is conducted with the robot prototype. In the experiment, a steel rope is suspended on a frame constructed with aluminium alloy extrusions, and an insulator chain, which is widely used for suspending the power transmission line, is set as a vertical obstacle for the robot. In the experiment, the wheel motor and three finger motors of the robot are all controlled manually with a wireless joystick, and a gyro sensor is fixed on the frame of module 2 to acquire the obliquity data of the robot body. The snapshots of the experiment process are shown in Fig. 11, and the obliquity variation of the robot body is shown in Fig. 12.

In the experiment process, when encountering the obstacle, the robot firstly stops and opens fingers of the front module and then goes on moving to make the front module cross the obstacle (Figs. 11(a) and (b) and stage 1 in Fig. 12). When the

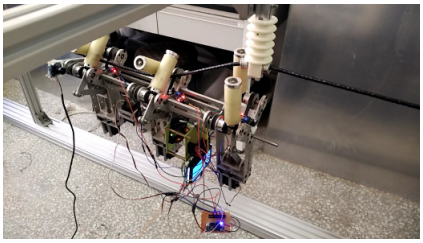

(a)

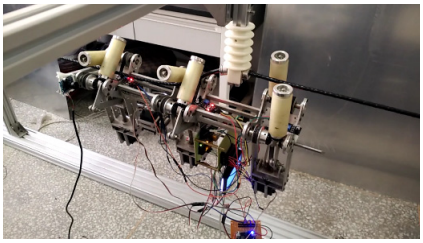

(b)

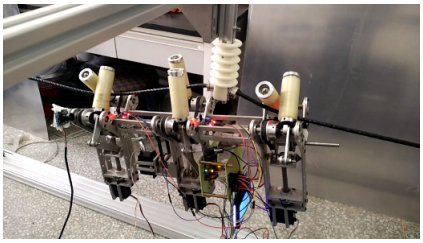

(c)

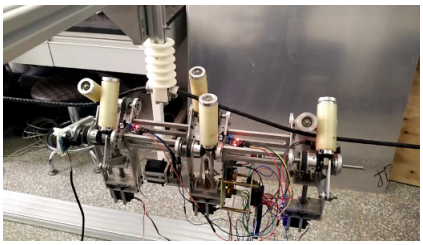

(d)

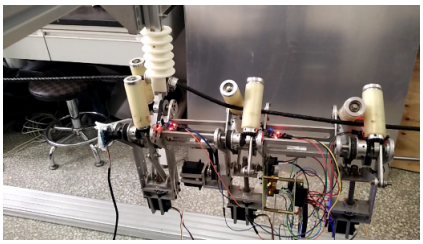

(e)

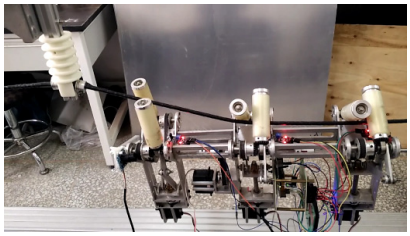

(f)

Fig. 11. Experiment snapshots.

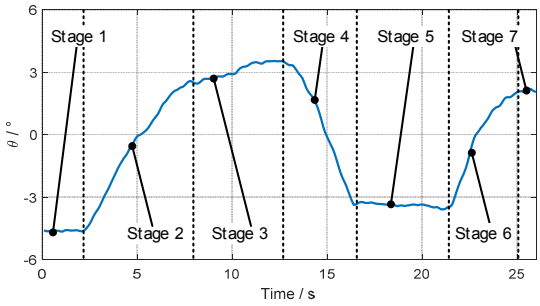

Fig. 12. Obliquity variation of robot body.

front module has crossed the obstacle, the robot stops and closes fingers of the front module and opens fingers of the middle module (Figs. 11(b) and (c) and stages 2 and 3 in Fig. 12). Then the robot goes on moving to make the middle module cross the obstacle (Figs. 11(c) and (d) and stages 4 in Fig. 12). When the middle module has crossed the obstacle, the robot stops and closes fingers of the middle module and opens fingers of the rear module (Figs. 11(d) and (e) and stages 5 and 6 in Fig. 12). Then the robot goes on moving to make the rear module cross the obstacle (Figs. 11(e) and (f) and stages 7 in Fig. 12). From the experiment result, it can be seen that the robot performs the obstacle-crossing process on the rope successfully, and this can give a verification for the rationality of the robot design and analysis work in this study.

7. Conclusions and future work

A modular rope-climbing robot with the finger-wheeled mechanism is proposed. The robot can achieve smooth and quick movement and obstacle-crossing on the rope and has a simpler mechanism compared with most of the existing rope-climbing robots. Moreover, the robot has a high adaptability for different rope environments and can be placed on the rope easily.

Aiming at three typical states during obstacle-crossing, the constraint equations of the robot are established through the geometric and force analysis, and the simulation based on established constraint equations and optimization calculating method presents the variations of the geometric variables and external forces exerting on the robot during obstacle-crossing that are used for the robot design work.

The robot prototype is developed based on the design and analysis work. The experiment for obstacle-crossing on the rope shows that the proposed robot performs the obstacle-crossing process successfully and gives a verification for the robot design and analysis work.

At this stage of the study, the motors of the robot (including three finger motors and a wheel motor) are all controlled manually, and this brings a problem that it is very difficult to realize the synchronous coordination control of all the motors, and the movement efficiency for obstacle-crossing of the robot is limited seriously. In the future work, the autonomous control of the robot will be studied.

Acknowledgments

This work is supported by National Natural Science Foundation of China (No. 52005348).

The authors wish to thank Fabing Yan and Yunfei Zang who are master candidates in the authors' laboratory for their contributions to the experiment work involved in this paper.

Nomenclature

L_{OAi} : Input displacement of slider A_i in Fig. 6
α_i : Rotation angle of link A_iB_i in Fig. 6
β_i : Rotation angle of the crank B_iC_i in Fig. 6
L_{hi} : Gripping height of the gripping module in Fig. 6
L_{si} : Intersection height of the crossing module in Fig. 6
L_{IJ} : Constant distances between points I and J in Fig. 6
L_W : Distance between adjacent modules in Fig. 7
L_H : Height of the module in Fig. 7
φ_i : Slope angle of each rope segment in Fig. 7
θ : Obliquity of the robot body in Fig. 7
θ_0 : Base obliquity of the gripping line in Fig. 7
θ' : Relative obliquity controlled by fingers in Fig. 7
N_i : Normal force from the rope in Fig. 8
F_i : Tangential force from the rope in Fig. 8
G : Gravity of the robot in Fig. 8

References

[1] F. Xu, J. L. Hu and G. P. Jiang, The obstacle-negotiation capability of rod-climbing robots and the improved mechanism design, *Journal of Mechanical Science and Technology*, 29 (7) (2015) 2975-2986.

[2] S. Han, J. Ahn and H. Moon, Remotely controlled prehensile locomotion of a two-module 3D pipe-climbing robot, *Journal of Mechanical Science and Technology*, 30 (4) (2016) 1878-1882.

[3] B. He et al., Mobility properties analyses of a wall climbing hexapod robot, *Journal of Mechanical Science and Technology*, 32 (3) (2018) 1333-1344.

[4] J. Gu, C. Wang and X. Wu, Self-adjusted adsorption strategy for an aircraft skin inspection robot, *Journal of Mechanical Science and Technology*, 32 (6) (2018) 2867-2975.

[5] A. B. Alhassan et al., Power transmission line inspection robots: A review, trends and challenges for future research, *International Journal of Electrical Power and Energy Systems*, 118 (2020) 1-19.

[6] K. Toussaint, N. Pouliot and S. Montambault, Transmission line maintenance robots capable of crossing obstacles: state-of-the-art review and challenges ahead, *Journal of Field Robotics*, 26 (5) (2009) 477-499.

[7] K. H. Cho et al., Caterpillar-based cable climbing robot for inspection of suspension bridge hanger rope, *Proc. IEEE International Conference on Automation Science and Engineering*, Madison, USA (2013) 1059-1062.

[8] G. R. Kanna and M. Ashik, Design and development of a rope

climbing robot using four bar mechanism with wireless control using TX2/RX2 RF module, *Proc. 2015 IEEE International Conference on Signal Processing, Informatics, Communication and Energy Systems*, Kozhikode, India (2015) 1-6.

[9] N. D. Hewapathirana et al., Analysis on four legged multi-purpose rope climbing robot, *Proc. International Conference on Industrial and Information Systems*, Sri Lanka (2019) 505-510.

[10] S. Urankar et al., Robo-sloth: a rope-climbing robot, *Proc. 11th National Conference on Machines and Mechanisms held at the Indian Institute of Technology*, New Delhi, India (2003) 1-10.

[11] P. R. Ratanghayra, A. A. Hayat and S. K. Saha, Design and analysis of spring-based rope climbing robot, *Machines, Mechanism and Robotics. Lecture Notes in Mechanical Engineering*. Springer, Singapore (2019) 453-462.

[12] D. Tandon, K. Patil and M. S. Dasgupta, Designing a modular rope climbing bot, *Proc. IEEE India Conference*, New Delhi, India (2016) 1-4.

[13] A. Fonseca, R. Abdo and J. Alberto, Robot for inspection of transmission lines, *Proc. 2nd International Conference on Applied Robotics for the Power Industry*, Zurich, Switzerland (2012) 83-87.

[14] L. Wang et al., Design, modeling and control of a biped line-walking robot, *International Journal of Advanced Robotic Systems*, 7 (4) (2011) 41-50.

[15] N. Morozovsky and T. Bewley, SkySweeper: a low DOF, dynamic high wire robot, *Proc. of IEEE/RSJ International Conference on Intelligent Robots and Systems*, Tokyo, Japan (2013) 2339-2344.

[16] W. Wang et al., Balance control of a novel power transmission line inspection robot, *Proc. of IEEE International Conference on Robotics and Biomimetics*, Zhuhai, China (2015) 1882-1887.

[17] S. Montambault and N. Pouliot, Field experience with LineScout Technology for live-line robotic inspection and maintenance of overhead transmission networks, *Proc. of 1st International Conference on Applied Robotics for the Power Industry*, Montreal, Canada (2010) 1-2.

[18] J. Wang et al., A new bionic structure of inspection robot for high voltage transmission line, *Proc. of 4th International Conference on Applied Robotics for the Power Industry*, Jinan, China (2016) 1-4.

[19] S. Wei et al., Design and validation of a novel robot for power lines inspection, *Proc. of IEEE International Conference on Information and Automation*, Lijiang, China (2015) 2683-2688.

[20] S. Y. Yu et al., Original design of a wheelchair robot equipped with variable geometry single tracked mechanisms, *International Journal of Robotics and Automation*, 30 (1) (2015) 87-97.

Suyang Yu is a Lecturer of the School of Mechatronics Engineering, Shenyang Aerospace University, Shenyang, China. He received his Ph.D. in Mechanical Engineering from Shenyang Institute of Automation, Chinese Academy of Sciences, China. His research interests include mobile robot and aerospace equipment.

Changlong Ye is a Professor of the School of Mechatronics Engineering, Shenyang Aerospace University, Shenyang, China. He received his Ph.D. in Mechanical Engineering from Shenyang Institute of Automation, Chinese Academy of Sciences, China. His research interests include Biorobotics and rescue robot.

Guanghong Tao is an Associate Professor of the School of Mechatronics Engineering, Shenyang Aerospace University, Shenyang, China. He received his Ph.D. in Mechanical Engineering from Northeastern University, China. His research interests include inspection robot, redundant robot, omnidirectional robot.

Jian Ding is a Lecturer of the School of Mechatronics Engineering, Shenyang Aerospace University, Shenyang, China. He received his Ph.D. in Mechanical Manufacturing from Harbin Institute of Technology, China. His research interests include parallel mechanism, digital manufacturing, and space automaton technology.

Yinchao Wang is a Lecturer of the School of Mechatronics Engineering, Shenyang Aerospace University, Shenyang, China. He received his Ph.D. in Mechanical Engineering from Harbin Institute of Technology, China. His research interests include intelligent robot, ultrasonic drilling sampling, and piezoelectric actuation.